ORIGINAL ARTICLE

Physical–chemical processes of sustainable materials' production from hazardous toner waste, galvanic glass waste and spent foundry sand

Vsevolod Mymrin[1] · Hélverton E. Ribas[1] · Daniela E. Pedroso[1] · Cleber L. Pedroso[1] · Walderson Klitzke[1] · Monica A. Avanci[1] · Alexandre J. Goncalves[1] · Paulo H. B. Rolim[1]

Abstract

Several sustainable white ceramic composites were prepared from 3 to 7 wt.% of hazardous toner waste, 30–40% of spent foundry sand, 15–25% of galvanic glass waste, and 35–45% kaolin clay. Developed composites were sintered at 1100°, 1150°, 1200°, 1250°, and 1275 °C. The ceramics' flexural resistance values reached up to 12.29 MPa, linear shrinkage varied between 2.99 and 11.20%, and water absorption—between 19.90 and 10.85%. The investigation of the ceramics structure formation processes using the X-ray diffraction, X-ray fluorescence, scanning electron microscopy, energy-dispersive spectroscopy, atomic absorption spectroscopy, and lased micro-mass analysis methods showed the synthesis of predominantly glassy structures with the inclusion of mullite and cristobalite crystalline structures. The analysis of the chemical composition of the gases emitted during ceramics firing at 1275 °C by the atomic absorption spectroscopy method, as well as the analyses of solubility and leaching of metals from ceramics sintered, showed that the developed composites and technology were in full compliance with Brazilian sanitary standards.

Introduction

The primary reason for the rise in the temperature of our planet atmosphere and the resulting growing number of environmental disasters that worry its population is the huge and constantly increasing quantity of industrial and municipal landfills that pollute the atmosphere, soil, surface and underground waters. A reasonable solution to this problem is to transform all those wastes into new sustainably and economically attractive raw materials.

Developed composites consist of three hazardous industrial waste—toner waste (TW), spent foundry sand (FS), and galvanic glass dust waste (GW) and natural kaolin clay. TW is not only harmful to health but also explosive. According to the [1], toner cartridges must be removed from any waste electrical and electronic equipment collected before recycling. TW is composed of small particles of a thermoplastic polymer containing carbon black or iron dioxide as a pigment (black toner), various organic pigments (color toner), and external additives such as wax, titanium dioxide, and silica [2]. Qualitatively similar to titanium dioxide, classified as carcinogenic, and comparable to asbestos, it can be irritating to people with respiratory conditions such as asthma or bronchitis [3].

International technical literature contains some number of papers on these wastes' utilization. Ruan and Xu [4, 5] have improved the eddy current separation (ECS) method for separating aluminum from plastic in crushed waste toner cartridge (TCs).

Gaikwad, et al. [6] completely transformed TW into a useful product using a temperature of 1550 °C, with an iron recovery of 81.6%. Kumar et al. [7] proposed the use of TW as a source of iron oxide; to recycle oil waste via hydrophobic sponge prepared from toner waste [8, 9], Huang, et al. used WT as an asphalt modifier for better engineering performance and cost-saving.

✉ Vsevolod Mymrin
  seva6219@gmail.com

1 Universidade Tecnológica Federal Do Paraná (UTFPR),
   av. Deputado Heitor Alencar Furtado, 4900, Sede Ecoville,
   Curitiba 81280-340, Brazil

[10] applied FS to develop environmentally clean construction materials from hazardous bauxite red mud. Guney et al. [11] replaced natural sand with FS by up to 15%; [11] evaluated its use as a substitute for fine aggregate in concrete production; FS was used with other industrial wastes [12], such as hazardous car paint waste [14] and galvanic Cr–Zn [15].

Glass waste is a waste of mechanical cleaning of metal objects with glass microspheres under the compressed air before they are electroplated with a thin layer of chromium, nickel or zinc. A large group of researchers used glass waste (GW) as a valuable binding component in materials' production: Jani et al. [16] used GW in cement and concrete; [17] applied it as cementing materials. Avila-Lopez et al. [18] researched binders containing GW and limestone. [19] added 10% GW to clay bricks and noticed a decrease of almost 100 °C in the firing temperature. Wei et al. [20] prepared lightweight aggregates from GW and coal fly ash.

Kaolin clay (KC) was the only natural component of this study. The reactivity of kaolin was explored by Emmanuel et al. [21] after NaOH activation. [21] revealed thermal reactions between kaolinite and calcite during alumina extraction from kaolin.

This overview of different methods for disposal of the industrial wastes used as raw materials in this research shows the scientific novelty of this paper and the originality of the developed method, because its objectives were: (1) to characterize the local hazardous industrial wastes, namely toner waste, galvanic glass waste, and spent foundry sand, here used as principal raw materials; (2) to develop sustainable ceramics from these waste with mechanical and physical properties corresponding to the demands of Brazilian technical and ecological standards; (3) to study the physical and chemical processes of the developed ceramics structure formation during their sintering at different temperatures.

Materials and methods

Raw materials and test samples (TSs) preparation

To decrease transportation cost of the developed ceramics, all raw materials were obtained from local industries in the city of Curitiba, Brazil. All test samples were prepared in pre-determined percentages, manually homogenized, hydrated, and compacted them.

Methods

All raw materials and developed ceramics were studied by the following methods: for the particle size distribution by laser diffraction; analysis of the particle size distribution by SALD-2300 Shimadzu analyzer dry method in combination with sew method; chemical composition by X-ray fluorescence (XRF) on a Philips/Panalytical. Micro-chemical composition has been studied in three complementary methods: (1) the energy-dispersive spectroscopy (EDS) method with an Oxford Penta FET-125 Precision; (2) by the lixiviation and solubility analyses using the atom absorption spectroscopy (AAS) method with a 4100 Perkin Elmer spectrometer; (3) isotopes' composition—by laser micro-mass analysis (LAMMA 1000). Mineral composition—by X-ray diffractometry (XRD) on a Philips PW1830; the results were interpreted with Super-Q X'Pert High Score Software. Changes of micro-morphological structure during ceramics' firing were studied by scanning electron microscopy (SEM) method. Three-points flexural resistance of the ceramics' test samples was carried out using the universal testing machine EMIC DL10,000; and linear shrinkage on Mitutoyo caliper; water absorption was determined by the weight increases after 24 h of total immersion in water.

Test samples were prepared in different pre-set percentages: toner waste (TW) variation: 0–7%; foundry sand (FS): 0–42%; glass waste (GW): 0–25% and kaolin clay (KC) 0–93%. The homogenized mixtures were hydrated with water content 12–19% and pressed with 5 MPa in a rectangular mold of 60 mm x 20 mm x 10 mm in size. The compacted samples were dried at 100 °C and burned for an hour at a 10 °C per minute heating rate ranging from 1100 °C to 1275 °C and unregulated furnace cooling.

Calculations

The linear shrinkage LS (%) values were obtained through the following equation:

$$LS = [(Li - Ls) / Li] \times 100 \tag{1}$$

where Li is the initial specimen length (mm), and Ls is the specimen length after sintering (mm).

The determination of the water absorption coefficients (C_{WA}) was carried out after ceramics' sintering using the following equation:

$$C_{WA} = [(M_{SAT} - M_D)/M_D] \times 100 \tag{2}$$

where M_{SAT} is the test sample mass after total water saturation for 24 h, and M_D is the dry test specimen mass.

Calcination loss (C.L.) values of the raw materials were obtained through the following equation:

$$C.L. = [(Wi - Ws) / Ws] \times 100 \tag{3}$$

where Wi is the initial specimen weight (gr), and Ws is the specimen weight after sintering for 1 h at 1000 °C (%).

Table 1 Raw materials' particle size distribution

Size (mm)	Toner waste	Foundry sand	Glass waste	Kaolin clay
More than 1.2	0.00	0.00	0.00	2.93
1.19–0.60	0.00	0.26	0.00	7.45
0.59–0.30	16.24	85.17	23.29	9.26
0.29–0.15	20.32	13.86	18.55	19.43
0.149–0.075	27.73	0.62	39.38	6.72
0.074–0.0	35.71	0.08	18.78	54.21

Research results

Raw materials' characterization

The raw materials were characterized by the particle size distribution, chemical and mineral compositions, and micro-morphological structure.

Particle size distribution of the raw materials

The natural kaolin clay presented the finest material (Table 1), containing the highest content (54.21%) of smaller particles (between 0 and 0.074 mm) followed by tonner waste (63.44%) of particles between 0 and 0.149 mm.

These results are comparable to those previously obtained by [22]. 39.38% of waste glass's particles was between 0.149 mm and 0.075 mm; 18.78% was smaller than 0.074 mm. 85.17% of the raw materials used in this research was foundry sand varying from 0.59 mm to 0.30 mm. The biggest part (39.38%) of waste glass's particles had size between 0.149 and 0.075 mm, 18.78% of particles is less than 0.074 mm.

Chemical composition of the raw materials by the XRF method

Chemical composition of the toner waste (TW) mainly consisted of SiO_2, Al_2O_3, TiO_2, and Fe_2O_3, with a total content of 41.02 wt.% (Table 2). All organic components of TW can explain such a high calcination loss value (C.L. = 46.07%). In addition, the results of studies AAS method (Table 3) also determined the presence of hazardous oxides such as PbO—3.30%, Cr_2O_3—0.90%, ZnO—0.08%, BaO—0.60%, and CuO—0.54% in TW (Table 3), which significantly exceeds the maximum permissible standards of Brazil [23]. Parthasarathy [24] informed that TW is one of the major electronic waste materials posing serious environmental threat and health hazards.

Globally, only about 20–30% of toner waste is recycled, while the remaining percentage is dumped in landfills. The

Table 2 Chemical composition of the raw materials (by the XRF method)

Oxides	Oxides' contents (wt. %)			
	TW	FS	GW	KC
SiO_2	19.30	89.06	77.47	47.16
Al_2O_3	10.04	4.02	0	36.20
TiO_2	7.70	0.25	0	<0.1
Fe_2O_3	3.90	1.06	0.20	0.43
CaO	0.08	0	8.35	0
K_2O	0.80	0.13	0.33	0.54
SO_3	0.90	1.03	0	0.65
Na_2O	0.43	0	10.16	0
MgO	0.40	0.32	3.04	0
C.L	46.07	4.15	0.45	15.02
Σ	100.00	100.00	100.00	100.00

World Health Organization has classified toner waste as class 2B carcinogen due to its potential health hazard. Considering the enormous volume of toner waste generated globally every year, better recycling and transformation strategies are needed immediately.

Spent foundry sand essentially contained SiO_2—89.06%, Al_2O_3—4.02%, with impurities of Fe_2O_3—1.06% and SO_3—1.03% and rather low C.L. = 4.15%. Glass waste had content of SiO_2 = 77.47%, CaO = 8.35%, Na_2O = 10.16%, and MgO = 3.04% with extremely low C.L. = 0.45%. As stated by [25], glass has similar general compositions, at least regarding the main oxides (SiO_2, Na_2O, and CaO).

Kaolin clay presented the plainest chemical composition (Table 1): 47.16% of SiO_2 and 36.20% of Al_2O_3. The high CL value (15.02%) is most likely due to the hydroxyl groups $(OH)_8$ of kaolinite $Al_4(Si_4O_{10})(OH)_8$ [27] and the pyrolysis of vegetable particles in the kaolin clay.

Mineral composition of the raw materials

The XRD pattern (Fig. 1) showed that the main minerals present in the toner waste were illite $2K_2O \cdot 3MgO \cdot Al_2O_3 \cdot 24SiO_2 \cdot 12H_2O$, titanium dioxide TiO_2 in the rutile and anatase phases, and quartz SiO_2. The stumpy maximum value of the crystalline peaks, noticed in TW's chemical composition, indicates a very high content of amorphous materials. The highest peak at $2\Theta° = 26.5°$ refers to coincident reflections of illite and quartz; however, the sum of their intensities was only 250–300 cps. Other minerals showed even lower intensity peaks.

Foundry sand (Fig. 1b) presented quartz SiO_2 and its high-temperature modification cristobalite quartz SiO_2. The amorphous phase quantity in FS is even higher than in TW because of the destruction of the quartz crystal structure by numerous thermal shocks in contact with molten iron. Part

Table 3 Results of leaching and solubility tests of the of the toner waste and developed ceramics composition 5 sintered at 1275 °C

Elements	Leaching, mg/L			Solubility, mg/L		
	TW	Comp. 5	[23]	TW	Comp. 5	[23]
As	3.24	<0.29	1.0	4.28	<0.001	0.01
Ba	0.60	<0.1	70.0	1.26	<0.1	0.7
Cd	1.39	<0.005	0.5	3.18	<0.005	0.005
Pb	3.30	<0.01	1.0	4.72	<0.01	0.01
Cr	0.90	<0.05	5.0	1.18	<0.05	0.05
Hg	1.83	<0.001	0.1	2.96	<0.0002	0.001
Se	2.14	<0.05	1.0	2.68	<0.01	0.01
Al	16.22	<0.10	*	18.27	<0.10	0.2
Cu	0.54	<0.05	*	1.20	<0.05	2.0
Fe	27.13	0.09	*	29.95	<0.05	0.3
Mn	15.62	<0.05	*	29.31	<0.05	0.1
Zn	0.08	<0.10	*	2.19	<0.10	5.0

Fig. 1 XRD patterns of the raw materials: **a** printer powder waste; **b** foundry sand; **c** glass waste and **d** kaolin clay
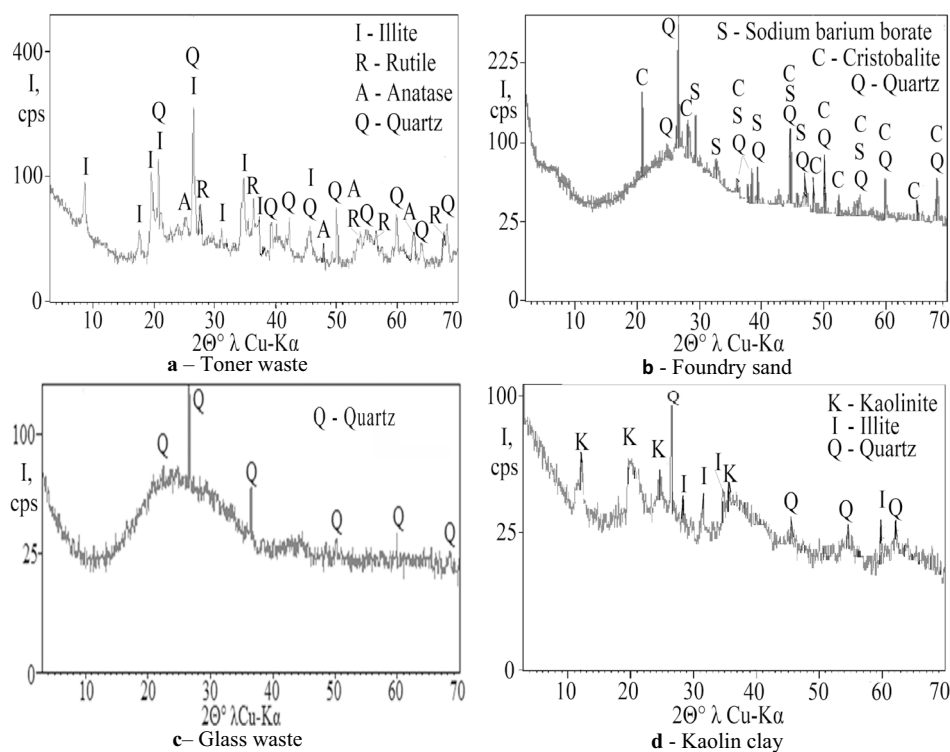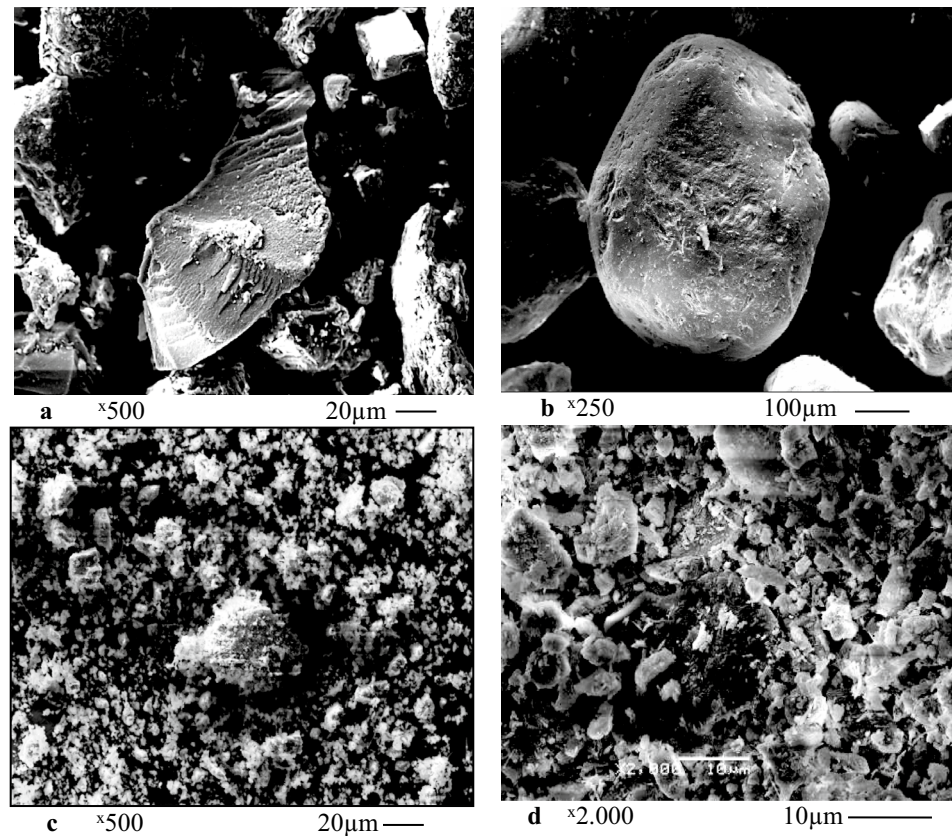
of the FS was melted, as evidenced by a structural X-ray halo, typical of glass, in the range of $2\Theta° = 12°–38°$. This halo makes it similar to glass waste (Fig. 2c) with a slight expansion range within $2\Theta° = 10°–40°$ due to the complete glass melting. FS, GW, and kaolin clay (Fig. 2d) showed resembling X-ray backgrounds (25cps), which indicates a relatively similar content of amorphous materials. Nevertheless, FS presented a higher amount of better-crystalized quartz and cristobalite with a peak intensity of 225 cps and higher. Kaolin clay comprised a small quantity of crystalized

kaolinite $Al_4(Si_4O_{10})(OH)_8$, illite $(K_{0.75}(H_3O)_{0.25})Al_2(Si_3Al)O_{10}((H_2O)_{0.75}(OH)_{0.25})_2$, and quartz SiO_2.

Micro-morphological structure of the raw materials

All raw materials had rather distinct morphological structures (Fig. 2) due to the significant difference in their origin and chemical composition. TW consists of irregularly shaped debris with sharp-angle particles of various sizes between 1 and 200 μm. Toner powder embodies several

Fig. 2 SEM micro-imagens of the raw materials: **a** toner waste, **b** foundry sand, **c** glass wastes, **d** kaolin clay

Developed materials' characterization

Flexural resistance of the developed materials

mixed ingredients made up of tiny particles that generally range from 5 to 15 microns.

FS is composed of rounded particles measuring between 100 and 700 µm; GW, like FS, also showed mainly rounded particles, but significantly smaller—from 1 to 60 µm; and the KC particles had a wide variety of forms—lamellar, needle-like, but mostly shapeless—with sizes from 1 to 15 µm.

The flexural resistance of ceramics made only with kaolin clay (Table 4, composition 1) increased from 2.41 to 5.10 MPa after firing at 1100° with decreasing till 2.95 MPa due to excessive melting of test samples at 1275 °C. The addition of 7% TW in kaolin clay (composition 8) increased the resistance from 3.49 to 12.29 MPa.

In order to determine the role of GW, its content was increased by 2% (compositions 5 and 4). Even with an

Table 4 Flexural resistance of the developed ceramics

Nº	Composition, wt.%				Flexural resistance (MPa) after T°C				
	TW	FS	GW	KC	1100	1150	1200	1250	1275
1	0	0	0	100	2.41	4.27	5.10	4.82	2.95
2	5	40	20	35	2.68	3.86	4.83	4.75	3.14
3	3	40	20	37	2.47	3.39	4.73	5.67	5.36
4	3	42	25	30	2.87	6.04	7.05	10.11	11.86
5	7	40	23	30	2.39	4.09	6.70	7.14	6.73
6	7	30	23	40	2.96	5.42	8.89	10.44	8.54
7	5	35	15	45	2.75	4.26	6.65	6.91	8.66
8	7	0	0	93	3.49	6.88	10.21	11.75	12.29
9	7	30	0	63	3.18	5.14	7.72	8.10	10.12

increase in FS amount at the expense of a sharp decrease in toner (to 3%), there was a robust increase in flexural resistance up to 11.86 MPa at 1275 °C, only lower than composition 8's resistance.

The KC influence was observed when comparing changes in flexural resistance of compositions 5 and 6 with equal amounts of TW (7%) and GW (23%) and with the replacement of 10% FS with 10% KC. The flexural resistance of ceramic 6 (40% clay) significantly exceeded the flexural resistance of ceramics 5 (30% clay), especially after firing at 1275 °C (10.44 versus 7.14 MPa). Above 1250 °C, both ceramics excessive melted, maintaining the difference in resistance, which was more noticeable at 1250 °C. Brazilian Technical Norm NBR 7170 [23] establishes that the value of flexural resistance for Class A solid bricks must be at least 2.5 MPa, for Class B, between 2.5 and 4 MPa and Class C, greater than 4 MPa.

Comparing the resistance of compositions 2 and 3 (equal amount of GW—20% and FS—40%), it was noted that the melting point of ceramics 2 (35% kaolin) and the onset of resistance loss was between 1200° and 1250°. For ceramics 3 (37% kaolin), the melting started between 1250 °C and 1275 °C due to the higher heat resistance of kaolinite and the lower melting point of TW with SiO_2 predominance in the chemical composition.

Linear shrinkage of the developed materials

Linear shrinkage values of all developed ceramics (Table 5) enlarged with increasing sintering temperature due to the chemical interaction processes between the components, melting some of them with compacting the pore volumes and shrinkage during the cooling.

Composition ceramics 8 showed the highest shrinkage values after sintering at all temperatures, followed by kaolin clay (composite 1). When studying the kaolin's interaction process with car paint waste, Mymrin et al. [14] obtained the opposite result—ceramics without industrial waste additives had the maximum shrinkage. This variance in results can

be justified by the high content of carbonates and vegetable remains in the kaolin clay used in the aforementioned research. The inclusion of 30–42% foundry sand drastically reduced (up to 2 times) the samples' shrinkage. Due to its relatively low chemical activity, the quartz sand presented in these mixtures played the role of a skeleton-forming component with low linear shrinkage at high temperatures in all composites (2–7 and 9), despite the high content of other components relatively active in them (TW, GW, and KC).

Water absorption of the developed materials

The water absorption values of the samples of all compositions (Table 6) decreased with the increase in the ceramic firing temperature and completely coincided with the change in flexural resistance and shrinkage of the samples (Tables 4 and 5). Shrinkage of samples with increasing temperature led to their compaction, decreased water absorption, and increased resistance. Therefore, the minimum water absorption (10.85%) and the maximum strength (12.29 MPa) after firing at 1275 °C were exhibited by ceramics 8. Ceramics of composition 1 had the second-lowest water absorption (11.38%) and very low resistance value (2.95 MPa) after firing at 1275 °C (Table 3).

Physical–chemical processes of the developed materials' structure formation

The study of the developed ceramic materials' structure formation processes was carried out on composition 5 because of their highest (7%) toner waste, almost highest (40%) FS and (23%) GW and the lowest (30%) kaolin clay content.

Changes in mineral composition of composite 5's samples during sintering

The comparison of the three diffractograms in Fig. 3 showed the complete change in the mineral composition of the initial mixture after firing at 1150 °C. Instead of the two clay

Table 5 Linear shrinkage of the test samples

Nº	Composition, wt.%				Linear shrinkage (%) after sintering at T°C				
	TW	FS	GW	KC	1100	1150	1200	1250	1275
1	0	0	0	100	4.28	4.33	7.01	7.22	7.24
2	5	40	20	35	3.24	4.89	5.42	5.98	6.14
3	3	40	20	37	2.99	4.26	5.10	6.01	6.55
4	3	42	25	30	3.15	4.01	4.99	5.87	6.96
5	7	40	23	30	3.56	4.03	4.37	5.10	6.28
6	7	30	23	40	4.10	5.11	5.77	6.24	6.86
7	5	35	15	45	3.75	4.11	4.76	5.84	6.04
8	7	0	0	93	6.2	6.98	8.12	10.45	11.20
9	7	30	0	63	4.17	4.85	5.10	5.28	5.54

Table 6 Water absorption of the ceramics after sintering

Nº	Composition, wt.%				Water absorption (wt.%) after T°C				
	TW	FS	GW	KC	1100	1150	1200	1250	1275
1	0	0	0	100	16.33	15.01	14.48	12.10	11.38
2	5	40	20	35	17.31	16.46	15.35	15.87	14.52
3	3	40	20	37	18.65	17.10	16.17	15.23	14.27
4	3	42	25	30	18.12	17.16	16.48	14.07	13.81
5	7	40	23	30	19.90	18.94	17.87	16.94	14.41
6	7	30	23	40	19.63	18.37	17.45	16.11	14.84
7	5	35	15	45	19.16	16.63	16.07	14.50	12.53
8	7	0	0	93	17.42	16.15	15.01	13.90	10.85
9	7	30	0	63	18.01	17.86	16.00	15.23	15.31

Fig. 3 XRD patterns of the composite 5: **a** initial dry mix; **b** ceramics sintered at 1150° and **c**—at 1275 °C
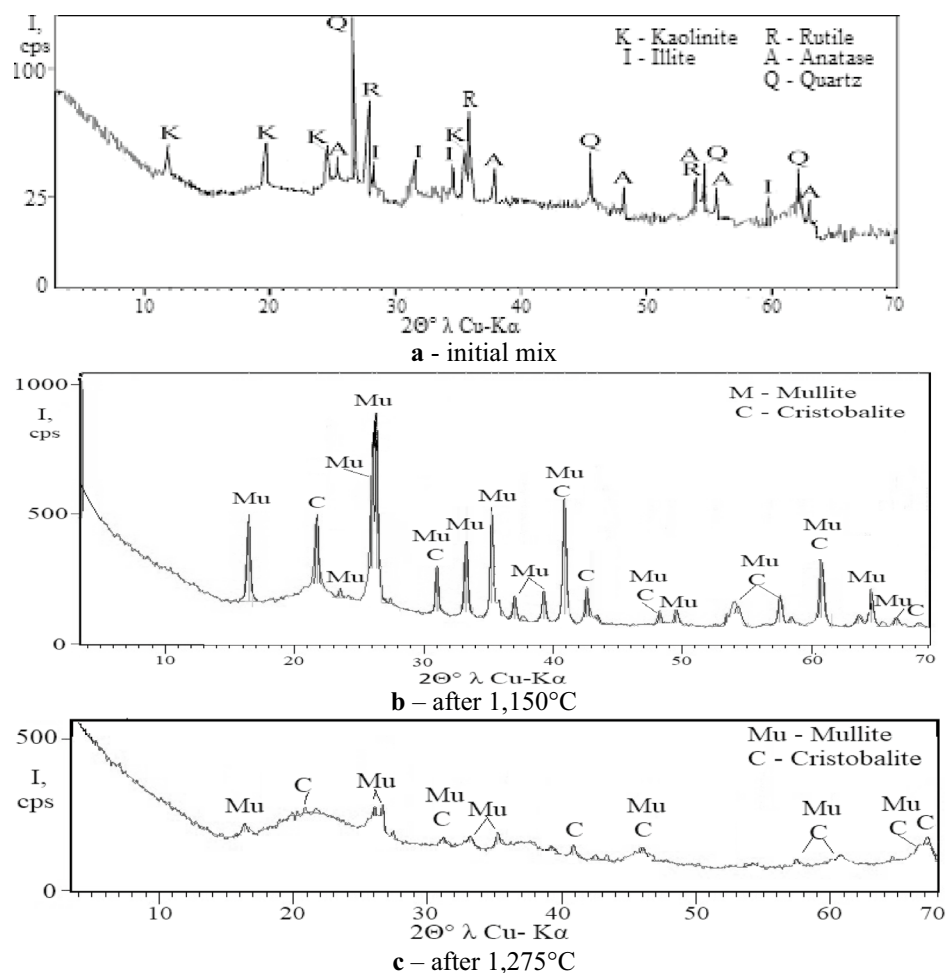
minerals (kaolinite and illite) and titanium dioxide TiO_2 (rutile and anatase), mullite was synthesized, and quartz was transformed into its high-temperature modification cristobalite. The intensity of the highest peak in the initial mix (Fig. 3a) slightly exceeded 100 cps (counts per second), while the remaining peaks of the crystalline phase of the initial mixture were slightly higher than the X-ray background of the amorphous phase.

After firing at 1150 °C (Fig. 3b), the mullite peak at $2\Theta° = 25°$ almost reached a height of 1000 cps, and the cristobalite peak at $2\Theta° = 22°$ achieved 500 cps. In this case, the X-ray background intensity also increased significantly, indicating a partial transition from the crystalline phase of the initial mixture to the amorphous state, apparently due to the melting at a temperature of 1150 °C.

When the ceramics were fired at 1275 °C (Fig. 3c), the opposite process occurred—the intensity of all peaks of the crystalline phase fell sharply and barely exceeded the X-ray background of the amorphous phase. This fact explains the reason for the almost end of the increase in flexural resistance of the test samples in this temperature range of 1250°–1275 °C (Table 4) from 7.14 to 6.73 MPa, which usually coincides the onset of excessive melting with a sudden drop in resistance. In the same temperature range, there was a very sharp decrease in the water absorption value (Table 6) from 16.94 to 14.41%, which also coincides with the increase in the amount of the amorphous melted phase filling the samples' pore space.

Changes in micromorphology of the test samples of composite 5

The analysis of the three micro-images of composition 5's structure at the same 5000-time magnification (Fig. 4) showed the transition stages from separate particles of different sizes and configurations of the initial dry mixture (Fig. 4a) to separate areas of fused and intergrown particles as a result of the firing at 1150 °C (Fig. 4b). Simultaneously, a large number of non-melted particles with large pores and cracks between them were still visible. Nevertheless, after firing at 1275 °C (Fig. 4c), almost the entire surface of the specimen was covered with a layer of new glassy formations, a large number of particles with a

diameter of 1 μm or less, similar to domes of non-emitted gases, and even smaller pores—gas exit channels were seen.

Large bumps and depressions between them indicate that the initial mixture's particles melted only superficially but not entirely throughout their volumes, explaining the sharp slowdown in the resistance increase (Table 4, composition 5). However, a further increase in the firing temperature 1275 °C inevitably led to the test samples' final melting.

Chemical composition of new formations by the EDS and LAMMA methods

The chemical composition of the new formations (Table 7) by the EDS method (Fig. 4c) demonstrated a very high heterogeneity of new formations' compositions, including the nearest points 1–3. The high carbon C content at all points can be attributed to vegetable residues in the clay and the high organic content in toner waste, such as styrene copolymer and acrylate, polyester resin, among others.

Similar results were obtained by the laser micro-mass spectroscopy (LAMMA) method (Fig. 5). All the closest points analyzed in ceramics 5 showed a significant difference from each other, both in terms of isotope set as their quantitative ratio.

Fig. 4 SEM micrographs from composite 5: **a** initial dry mix; **b** ceramics sintered at 1150° and **c**—at 1275 °C
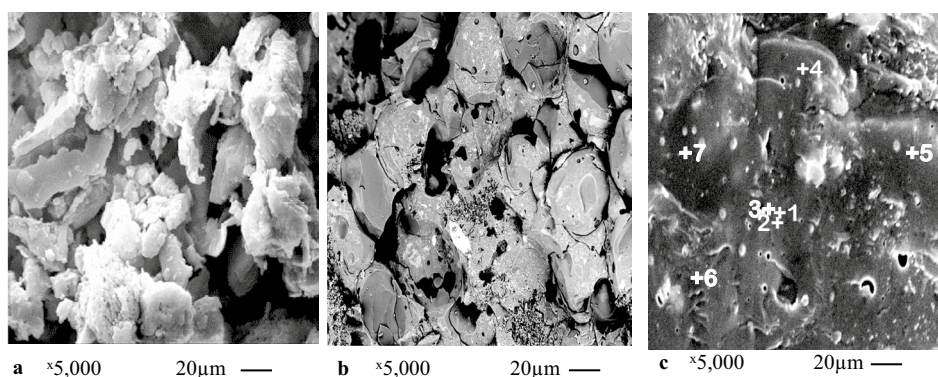
a   ×5,000   20μm ——   b   ×5,000   20μm ——   c   ×5,000   20μm ——

Table 7 Chemical compositions of the new formations of ceramics 5 (by the EDS method, Fig. 4c) after sintering at 1275 °C

Chemical elements	Chemical elements contents (wt.%) of the points						
	1	2	3	4	5	6	7
C	24.58	36.92	25.94	38.72	23.87	26.81	28.84
Al	39.74	27.77	18.88	40.19	24.49	32.35	27.83
Si	26.66	24.56	43.28	19.79	51.64	29.97	34.99
Fe	3.88	6.90	5.47	0	0	10.71	0
Ti	5.14	3.85	6.13	10.30	0	0	8.34
Ca	0	0	0.30	0	0	0.16	0
Σ	100.00	100.00	100.00	100.00	100.00	100.00	100.00

Fig. 5 Isotope's composition of the new formations of ceramics 5 (by the LAMMA method) after sintering at 1275 °C
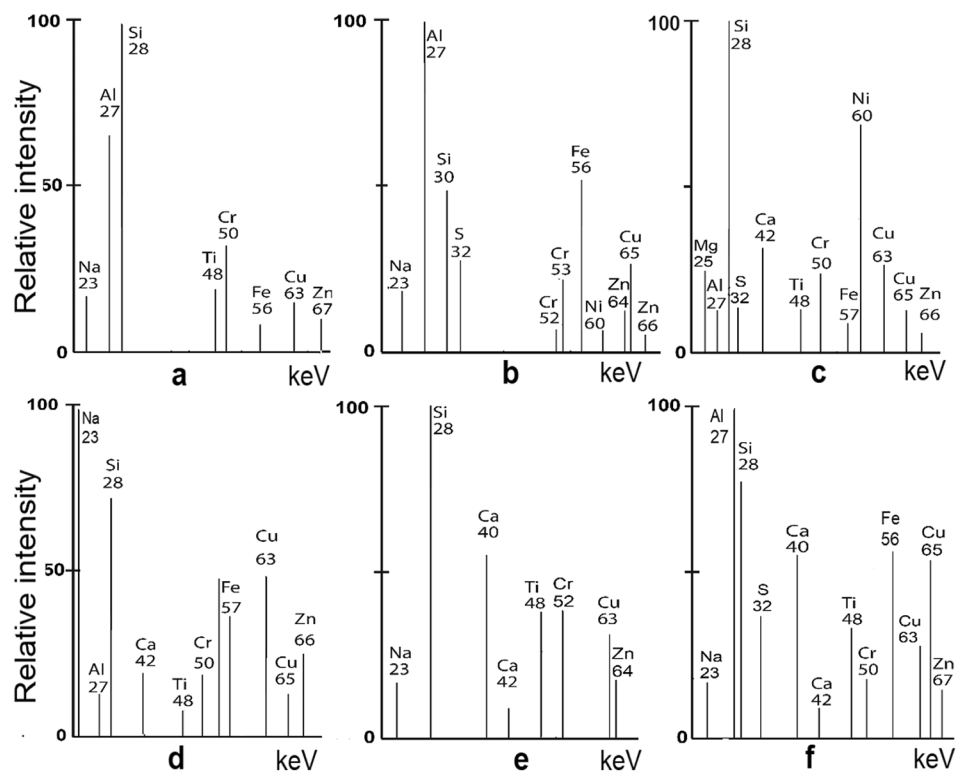
Environmental properties of the developed materials

Leaching and solubility of the developed materials in acid solutions

The chemical composition of the toner waste (TW), determined by the AAS method (Table 3), indicated the presence of hazardous oxides such as PbO—3.30%, Cr_2O_3—0.90%, ZnO—0.08%, BaO—0.60%, and CuO—0.50%, and with 1% of ZrO_2, NiO, MoO_3, Co_3O_4, and SrO in TW. The results obtained by the LAMMA method (Fig. 5) also confirmed the presence of heavy metals (Cr, Cu, and Zn) in the ceramics. Therefore, it became necessary to investigate the developed materials' environmental properties and the gases formed during their firing.

The maximum of hazardous TW content is 7% in compositions 5 and 6 (Table 4), but the composition 5 was chosen to study the developed ceramic's environmental characteristics due to its higher (40%) hazardous FS and 30% ecologically pure KC contents; composition 6 has 30% FS and 40% KC. The obtained results demonstrate (Table 3) full compliance of leaching and solubility tests of ceramics 5 with the Brazilian sanitary standards [26].

Gas emission during ceramics sintering

Samples of the heat gases were collected during ceramics' sintering at 1275 °C in the glass filter (Fig. 6) with a thickness of 0.45 μm. The separation of the solid particles deposited on the filter was performed by ultrasound (for
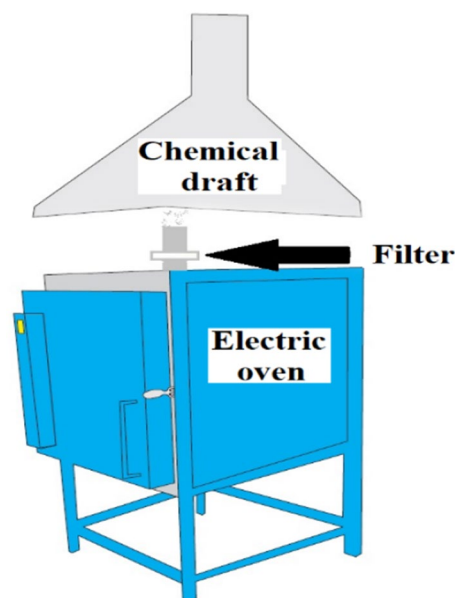
Fig. 6 Electric oven with gas filter

Table 8 Gas emission rates during the sintering of the developed ceramic

Heavy metals	Compositions, mg/Nm³	[26], mg/Nm³
Cu	2.150	5.0
Cd	0.074	0.2
Pb	0.103	5.0
Cr	0.159	5.0
Ni	0.061	1.0
Zn	1.473	5.0

three hours in an acidic medium) and determined by the AAS method (Table 8). The washing of all glassware and vitreous filters (Fig. 6) with heavy metals (Cr, Zn, and Pb), Sn, Ni and others (Fe, Al, etc.) was carried out by soaking them for a minimum of 24 h in nitric acid (HNO_3) with concentration 10%. The concentration of heavy metals of the resulting solution was analyzed with the 4100 Perkin Elmer spectrometer.

Comparison of the values of leaching and solubility tests of the ceramics Comp. 5 with toner waste shows their leaching reduction after firing at 1275 °C compared to the Brazilian HBP standards by 700 times for Ba, 200 times for Se and 100 times for Cd, Cr and Hg, indicating their strong bonding with glassy new formations.

Comparison of the output values of heavy metals with hot gases during sintering of the ceramics shows much worse performance compared to the standard norms of Brazil. For example, the output of Cu with gas is only 2.4 times lower than the permissible norm, the output of Cd is 2.7 times, Pb is 48.5 times, Cr is 31.4 times, Ni is 16.4 times, and Zn is 3.5 times. Obviously, this difference compared to the values of leaching and solubility of heavy metals from the ceramics in acid solutions (Table 3) is due to the increased carryover of heavy metals at low temperatures since the beginning of sintering. Industrial firing of ceramics is carried out by continuous movement of a conveyor with materials into a high-temperature kiln. Therefore, in the production process of firing, the removal of heavy metals should be noticeably lower than laboratory conditions with slow (5 °C per minute) heating of the furnace.

Conclusions

1. The feasibility of using hazardous toner dust waste in compositions with spent foundry sand, glass waste, and kaolin clay for the production of environmentally friendly ceramic materials has been experimentally proven. The scientific novelty of this paper is development of new sustainable ceramics composites from 3 to 7 wt.% of hazardous toner waste, 15–25% of galvanic glass waste, 30–40% of spent foundry sand, and 35–45% kaolin clay.

2. Flexural resistance of the developed materials reached up to 12.29 MPa, linear shrinkage varied between 2.99 and 11.20%; water absorption—between 19.90 and 10.85%.

3. The investigation of the physicochemical processes of the developed materials' structure formation by the XRD, SEM with EDS, LAMMA, and AAS methods showed complete decomposition of initial crystal structures of the initial components (kaolinite, illite, rutile, anatase, sodium–barium borate and quartz) and synthesis of the predominantly amorphous glassy structures with the inclusion of small quantities of mullite and cristobalite.

4. Environmental properties of the developed ceramics were controlled by the gases emitted during the ceramics firing study and by solubility and leaching of metals in acid solutions. The results obtained by both methods confirmed their sustainability during production and application as construction materials. Therefore, their life cycle can be prolonged as environmentally clean raw materials to produce new construction materials.

Declaration

References

1. EU Directive 2002/96 / EC https://www.urt-recycling.com/seite/en/disposal/053/-Recycling_of_toner_aartridges .html4

2. Fukumaru M et al (2015) Titanium dioxide as external additive for ton. J Imaging Soc Japan 54:148–152. https://doi.org/10.11370/isj.54.148

3. Powell A (2018) At Harvard Chan School. Nano safety is no small concern (interview with Philip Demokritou. https://news.harvard.edu/gazette/story/2018/10/at-harvard-chan-school-nano-safety-is-no-small-concern/

4. Ruan J, Xu Z (2011) An environmentally friendly recovery production line of waste toner cartridges. J Haz Mat 185:696–702. https://doi.org/10.1016/j.jhazmat.2010.09.074

5. Ruan J, Xu Z (2011) A new model of repulsive force in eddy current separation for recovering waste toner cartridges. J Haz Mat 192:307–313. https://doi.org/10.1016/j.jhazmat.2011.05.025

6. Gaikwad V et al (2017) Thermal transformation of waste toner powder into a value-added ferrous. J ACS Sust Chem Eng 5:11543–11550. https://doi.org/10.1021/acssuschemeng.7b02875

7. Kumar U et al (2018) Transformation of waste toner to iron using E-waste plastics as a carbon resource. J Cle Prod 192:244–251. https://doi.org/10.1016/j.jclepro.2018.05.010

8. Shi P et al (2018) Recycle of oil waste via hydrophobic sponge prepared from toner waste. J Haz Mat 360:615–622. https://doi.org/10.1016/j.jhazmat.2018.08.052

9. Huang J et al (2021) Rheological properties of bituminous binder modified with recycled waste toner. J Cle Pro 317:128415. https://doi.org/10.1016/j.jclepro.2021.128415

10. Alekseev K et al (2019) Environmentally clean construction materials from hazardous bauxite waste red mud and spent foundry sand. J Con Build Mat 229:116860. https://doi.org/10.1016/j.conbuildmat.2019.116860

11. Guney Y et al (2010) Re-usage of waste foundry sand in high-strength concrete. J Waste Man 30:1705–1713. https://doi.org/10.1016/j.wasman.2010.02

12. Prabhu GG et al (2014) Effects of foundry sand as a fine aggregate in concrete production. J Con Build Mat 70:514–521. https://doi.org/10.1016/j.conbuildmat.2014.07.070

13. Mastella MA et al (2014) Mechanical and toxicological evaluation of concrete artifacts containing waste foundry sand. J Waste Man 34:1495–1500. https://doi.org/10.1016/j.wasman.2014.02.001

14. Mymrin V et al (2019) Manufacturing of sustainable ceramics with improved mechanical properties from hazardous car paint waste to prevent environmental pollution. Int J Adv Man Tech 105:1–1. https://doi.org/10.1007/s00170-019-04302-z

15. Mymrin V et al (2020) Galvanic Cr-Zn and spent foundry sand wastes application as valuable components of sustainable ceramics to prevent environment pollution. J Adv Man Tech 107:1239–1250. https://doi.org/10.1007/s00170-020-05066-7

16. Jani Y, Hogland W (2014) Waste glass in the production of cement and concrete–a review. J Env Chem Eng 2:1767–1775. https://doi.org/10.1016/j.jece.2014.03.016

17. Bignozzi MC et al (2015) Glass waste as supplementary cementing materials: the effects of glass chemical composition. J Cem Con Comp 55:45–52. https://doi.org/10.1016/j.cemconcomp.2014.07.020

18. Avila-López U et al (2015) Investigation of novel waste glass and limestone binders using statistical methods. J Con Build Mat 82:296–303. https://doi.org/10.1016/j.conbuildmat.2015.02.085

19. Phonphuak N et al (2016) Utilization of waste glass to enhance physical–mechanical properties of fired clay brick. J Clean Prod 112:3057–3062. https://doi.org/10.1016/j.jclepro.2015.10.084

20. Wei Y-L et al (2016) Effect of waste glass addition on lightweight aggregates prepared from F-class coal fly ash. J Con Build Mat 112:773–782. https://doi.org/10.1016/j.conbuildmat.2016.02.147

21. Emmanuel E et al (2019) Insights on the clay reactivity in alkaline media: Beyond filler role for kaolin. J App Clay Sci 181:105210. https://doi.org/10.1016/j.clay.2019.105210

22. El-Deeb AB et al (2020) Solid state and phase transformation mechanism of kaolin sintered with limestone for alumina extraction. J App Clay Sci 196:105771. https://doi.org/10.1016/j.clay.2020.105771

23. Nakamura Y, Kutsuwada N (1989) Direct measurement of toner particle size. J Mat Sci. https://doi.org/10.1109/IAS.1989.96951

24. NBR 10,004 (2004) Solid Waste Classification, Rio de Janeiro.

25. Parthasarathy M (2021) Challenges and Emerging Trends in Toner Waste Recycling: A Review. J Recycling 6:57. https://doi.org/10.3390/recycling6030057

26. Menchaca-Ballinas LD, Escalante-García JI (2020) Limestone as aggregate and precursor in binders of waste glass activated by CaO and NaOH. J Con Build Mat 262:120013. https://doi.org/10.1016/j.conbuildmat.2020.120013

27. Vereecken E et al (2020) Does kaolin clay really create a perfect hydraulic interface contact between materials? J Con Build Mat 262:120700. https://doi.org/10.1016/j.conbuildmat.2020.120700

28. NBR 7170 – Ceramic Solid Brick Masonry Specification, in ABNT – EB-19/1983: Solid Brick Origin Description - CB-02 Brazilian Civil Construction Committee